

Hardening Effects of In-Situ Aging for a Laser Welded Maraging Steel

Milton Sergio Fernandes de Lima, Rafael Humberto de Mota Siqueira,
Sheila Medeiros de Carvalho and Antonio Jorge Abdalla

Photonics Division, Institute for Advanced Studies, 12.228-001 São Jose dos Campos, Brazil

Article history

Received: 07-10-2019

Revised: 06-11-2019

Accepted: 11-11-2019

Corresponding Author:

Milton Sergio Fernandes de
Lima

Photonics Division, Institute for
Advanced Studies, 12.228-001
São Jose dos Campos, Brazil
Email: msflima@gmail.com

Abstract: Maraging steels are ultra-high strength alloys which have been successfully laser welded to obtain structural components. For most of the applications these steels are in an aged state to attain tensile strength up to 1.5 GPa, although welding induces local softening due to dissolution of precipitates. This paper aims to investigate the effect of in-situ aging of the maraging steel plates after laser welding to reduce the local softening. For a preheating at 40°C, just below the martensite finish line, the hardness of the Fusion Zone (FZ) attained between 440 and 490 HV and the Heat-Affected Zone (HAZ) attained a maximum of 570 HV compared to 300 HV of the Base Material (BM) for aging temperatures between 450°C and 520°C and periods between 10 and 30 min. The intercritical aging (570°C/1 h) also promoted an increase in local hardness of FZ 320 HV and HAZ 400 HV. Using an intercritical aging, the hardness situated between room temperature and quenched and aged coupons and was more homogeneous considering FZ, HAZ and BM. The microstructure of the intercritical aged welds is marked by duplex-ferrite and martensite micro-constituents.

Keywords: Maraging Steels, Laser Beam Welding, Post-Welding Heat Treatment, Aging

Introduction

Maraging alloys belong to the Ultra-High Mechanical Strength Steels (UHSS) as could attain tensile strengths up to 3.4 GPa depending on composition and the thermo-mechanical treatments (Rohrbach and Schmidt, 1993). Different from ordinary UHSS, Maraging steel martensite is ductile and the maximum strength is obtained by aging (Silva *et al.*, 2019). The phase transformations for produce the steel ingots are the origin of the name MARtensite and AGING. Bieber (1969) was the first to prove that a Fe-25%Ni-4%Ti-4%Al steel attained a maximum tensile strength of 1 GPa after aging at 480°C during 160 min.

Although Maraging steels proved their usefulness in high demanding applications such as rocket bodies, high pressure tanks and landing gears, welding is still a challenge (Rajkumar *et al.*, 2014). Fusion welds solubilizes the precipitates into the austenite matrix and produce softened weld zones (Fanton *et al.*, 2014). Even with solid state processes failed to prevent softening of the joint because annealing produces fully martensite in cooling (Kellogg, 2012).

Silva *et al.* (2019) heat treated a class 300 Maraging steel from 1 to 100 h at 440°C obtaining hardness ranging from 300 HV to 620 HV. These authors recorded the Moessbauer spectra for each aging time and noted that a high mobility of Mo and Ti atoms for times under 3 h.

The present investigation proposes an inductive heating together with the laser weld of Maraging 300 steels in order to produce aging directly in the final product. One difference of the current approach to the conventional heat treating is that the material is not normalized prior to aging. It is expected that Base Material (BM) and the Heat-Affected Zone (HAZ) austenitize rapidly during laser heating. However, the Fusion Zone (FZ) of the welds present microsegregation which will produce composition modulations retained during aging. These assumptions are corroborated by Casati *et al.* (2016).

Inductive heating in laser welding had been already used to increase the cooling period of EN 10025-6 S690QL fine-grained structural steel (Lahdo *et al.*, 2014) and to produce bainite in hot-stamping steels (Lima *et al.*,

2017). However, to the best knowledge of the authors, it is the first time aging is applied concomitant to laser welding of maraging steels.

Krasnikova *et al.* (1986) reported that the interdendritic region of as-cast ingots of 250 maraging are rich in Ti and Mo. These segregations induce the formation of δ -ferrite precipitates and to a depletion of these elements in the dendrite trunks. Linnert (1967) stated that reducing these elements in the Fe-Ni tempered martensite reduces the mechanical strength due to a decrease in precipitation hardening potential. These findings were also pointed out by Pektaş and Atala (1998) which indicated a high temperature solution treatment, e.g., 1000°C/4h, aiming to reduce the elements segregation.

The temperatures for the isothermal treatment, i.e., 450°C, 480°C e 520°C, were determined in a previous study (Lombardo *et al.*, 2016). According to Pektaş and Atala (1998), 18%Ni maraging steels present a good balance between tensile strength and toughness when aged at 480°C per 4 h. The maximum temperature of austenite precipitation was chosen according to Kapoor *et al.* (2003) at 570°C as the maximum density of precipitates measured by dilatometric tests in 18wt.% Ni maraging steel of grade 350.

One way to understand the martensitic transformation in maraging steels is to start with the metastable phase diagram, Fig. 1. From the solidification, there is no transformation of the austenite phase in the steel before it reaches the Martensite Start (Ms) temperature. Some studies show that the martensitic transformation always operates on 300 maraging steels, even when the cooling

rate is quite slow, as well as in large parts. The resulting martensite has a center body cubic structure, as opposed to the hexagonal structure of the common martensites of the steels, due to the low carbon content. Martensite is relatively ductile, 0 ~ 30 HRC and has a high dislocation density without significant twining. Alloy elements change Ms but do not alter the fact that the martensitic transformation is independent of the cooling rate (ASM Handbook Committee, 1990a). The great majority of the alloying elements and in particular the Ni, decrease the transformation temperature Ms. Cobalt is an exception because it increases Ms. The addition of Co is precisely to balance the decrease in Ms of the alloying elements, e.g., Ni, Ti, Mo, which are required for precipitation during aging.

According to common practice, aging hardening is carried out at temperatures between 455 and 510°C for 3 to 9 h, followed by air cooling. From the phase diagram, blue lines in Fig. 1, 42% of ferrite is obtained for an 18.5% Ni composition and a temperature of 500°C. A reversion to an austenitic-ferrite structure would hinder precipitation hardening. However, the enthalpy for precipitation of intermetallic phases is smaller than the reversal for a ferrite-austenite mixture. For example, for the current alloy and according to ThermoCalc computations, the equilibrium phases at 475°C are: Iron ferrite (92% mole), Ni₃Ti (3% mole), FeCr (3% mole) and Cu_{0.76}Ti_{0.23} (1% mole) (Sha, 2000). Therefore, there is a precipitation of phases inside the grains with martensitic structure in plates aided greatly by the high density of dislocations. The distribution of particles consistent with the matrix is uniform and the main hardeners are Ti-based.

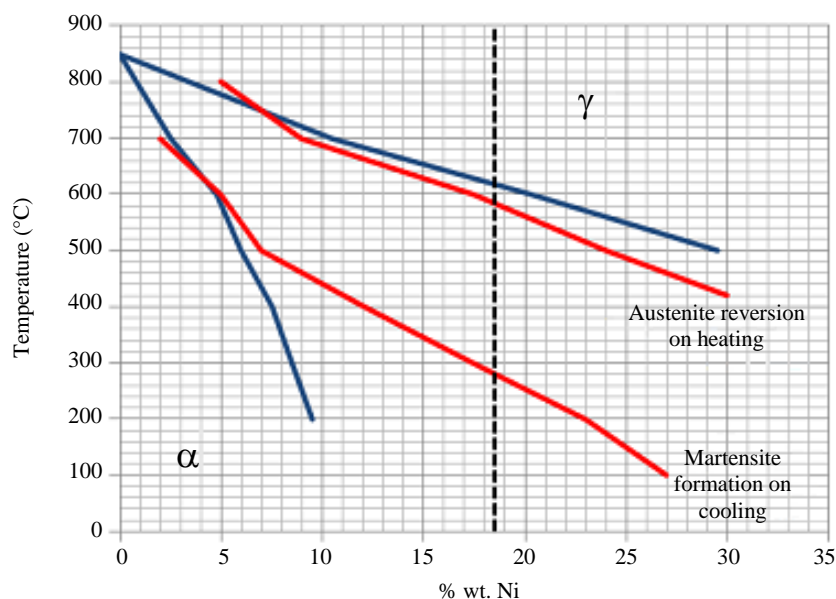


Fig. 1: Pseudobinary phase diagram for the solid state transformations in Maraging 300 steel (ASM Handbook Committee, 1990a)

The phase with the least distortion (misfit) in the CCC matrix of martensite is Ni_3Ti and therefore privileged in the initial states. The precipitation has a limit given by the solute diffusivities and high aging times tend to form the so-called reversed austenite. Overaging causes an expressive reduction of the hardness of the steel and is fundamentally the reversion to the thermodynamic equilibrium in the intercritical zone (Fig. 1). The most probable mechanism of reversed austenite formation is the dissolution of nickel-rich precipitates, which enriches the matrix and renders the austenite more thermodynamically stable. The red lines in Fig. 1 presents the experimental limits (ASM Handbook Committee, 1990a) for Austenite reversion on Heating (Ah) and Martensite formation on Cooling (Mc) together with the current initial Ni composition.

Experimental

The material was received as an 18%Ni class 300 Maraging steel from Böhler Co. in the form of 3.3 mm thick plates. The composition is given in Table 1 and agrees with the SAE AMS 6514F standard (SAE Mobilus, 2019). The material was hot rolled and air-cooled resulting in a relatively soft martensite (330 HV).

The laser workstation is composed of an YLR-2000 IPG Photonics fiber Laser, a CNC table, a furnace and auxiliary systems. The laser minimum spot is 0.1 mm and the beam quality is $M^2 = 9$. The CNC table is driven by three step motors with maximum speed of 160 mm/s and processing area of $400 \times 500 \text{ mm}^2$. The furnace was conceived for inductive heating during the welds as previously reported in the literature (Lima *et al.*, 2017). The auxiliary systems comprise water cooled jackets and nitrogen cross jet to protect the optics.

The welds were realized bead-on-plate with the focus on the top of the upper surface. The surfaces were grounded and cleaned with ethanol prior to the welds. After the focus position was calibrated $50 \times 50 \text{ mm}^2$ samples of the steel were positioned in the center of the furnace. The samples were inductively heated up to a given temperature and maintained at these temperatures with the use of a manual switch. One thermocouple welded to the bottom surface of the plate recorded the temperature profile. The furnace and laser setup were reported elsewhere (Braga *et al.*, 2018).

Since the steel plates were inserted in a furnace, a protective atmosphere was not possible. However, previous results have shown that the porosity due to the atmospheric contamination is high only for full penetration welds, i.e. when the fusion zone attains the lower surface of the plate. In view of this, the laser power and weld speed were conceived for partial penetration. For the current experimental conditions, the laser power was fixed at 1800 W and the weld speeds were 1.8, 2.4 and 3.0 m/min in accordance to a previous work (Sakai *et al.*, 2015).

Table 1: Chemical composition of the base material (wt.%).
 Fe as the balance

C	Si	Mn	Ni	Mo	Co	Al	Ti
0.005	0.05	0.05	18.5	5.0	8.8	0.11	0.70

The microstructure of the samples was analyzed by a Light Optical Microscopy (LOM) using an Imager.2M Zeiss microscope and Nital 2% etching. Scanning electron microscopy was carried out using a Hitachi TM-3000 microscope. An equipment model FM800 (Futuretech) was used for Vickers hardness tests using 100 gf load and a dwell time of 10 seconds.

For thermodynamic calculations using the ThermoCalc© software, the TCFE6-steel database was used (Andersson *et al.*, 2002). The thermal simulation was carried out using Sysweld© Software (Esi-Group, 2019). Sysweld is a Finite Element Modeling (FEM) software specially designed for welding and heat treatment of metals and alloys. For the current purpose a mesh refined around the laser path was designed with a lateral resolution of about 0.001 mm. The exact maraging 300 properties are not available in the Sysweld database, therefore X5CrNi1810 (EN 1.4301) steel properties were used instead. The model dimensions and welding procedure followed those described in the experimental design, starting with the material at room temperature and heating it up to a given temperature T^* . The software produces many valuable outputs, but those of interest here are the time-temperature evolution in different regions of the plate.

Results and Discussion

Ambient Temperature Welds

Figure 2 presents cross-section images of representative welds obtained for speeds of 1.8, 2.4 and 3.0 m/min. In a general view, the welds were thinner and deeper as the speed varies from 1.8 to 3.0 m/min. The weld obtained at 1.8 m/min has a top width of 2.2 mm and penetration of 2.5 mm, compared to the weld obtained at 3.0 m/min with a top width of 1.2 mm and penetration of 2.7 mm. As the welds were performed without gaseous protection, the plasma generated on the surface of the plate is more intense with slower speed, since the interaction time increases and more metallic ions are present. Additionally, as speed increases, the plasma plume tends to move back from the center of the keyhole, allowing the incident beam to penetrate further into the plate. This effect is known and reported as a function of the gas flow, causing the plasma to move away from the center of the beam (Joseph *et al.*, 2017).

The extent of HAZ is a function of the welding speed, although it varies depending on the region where it is measured. In the case of the macrographs shown in Fig. 2 the HAZ ranges between 0.7 and 0.4 mm, from

1.8 to 3.0 m/min. This region is equivalent to the limit of dissolution of intermetallic precipitates responsible for the hardening of the material. From the FEM simulations, the limit of the HAZ represents an isotherm of 900°C.

It is expected that microsegregation appears among the dendritic branches of the fusion zone (Fig. 3). In the figure, the central region is composed of equiaxed dendrites spaced 3 μm and where 39% were interdendritic material. These values did not change significantly in the current speed interval.

Figure 4 presents the time-temperature profile for each speed condition estimated in the middle of the fusion zone. Each curve is displaced in time for better visualization. According to the thermodynamic database Thermocalc (Andersson *et al.*, 2002), the liquidus temperature is 1417°C, also displayed in Fig. 4. For every condition, the liquid was superheated above 1900°C and the cooling rates at liquidus were estimated

16'300, 22'500, 25'700°C/s for 1.8, 2.4 and 3.0 m/min, respectively. Near to 760°C, the cooling rates are 4'000, 5'700, 6'900°C/s for 1.8, 2.4 and 3.0 m/min, respectively, which are large enough to produce martensite transformation with a Vickers hardness of 313 HV (ASM Handbook Committee, 1990b).

The actual hardness profiles of the samples are presented in Fig. 5. The Fusion Zone (FZ) hardness (open squares in Fig. 5) situated between 280 and 300 HV, consistent with an unaged martensite structure. The Heat-Affected Zone (HAZ) hardness (crossed-squares in Fig. 5) is typically above the FZ Vickers hardness because of the solid-state transformation implies in the absence of microsegregation. Finally, the Base Material (BM) is delimited by the temperature below the austenite reversion on heating (Fig. 1). The rise in HV for the BM near to the HAZ is due to local ageing of the original martensite.

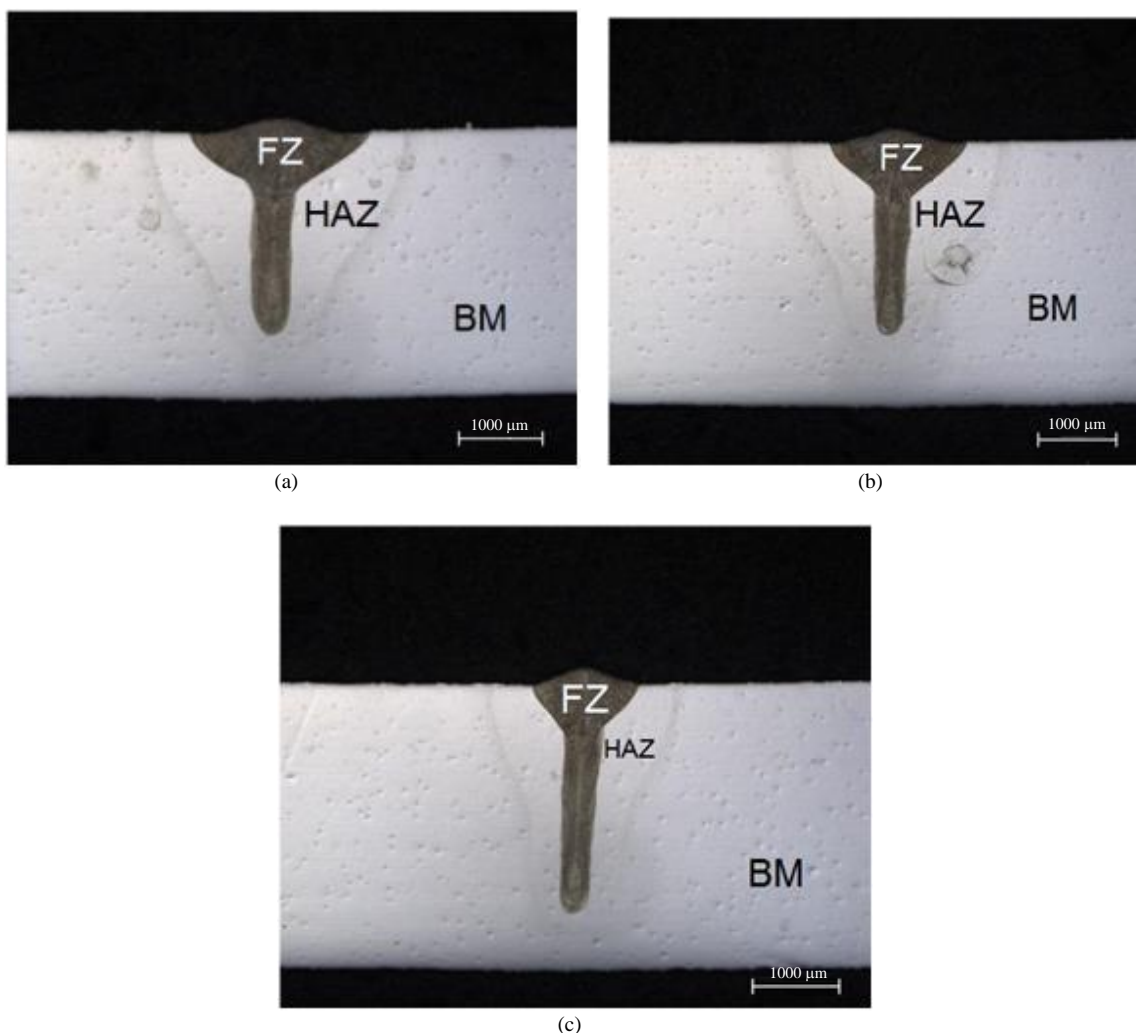


Fig. 2: Macroscopic view of the welds at different speeds: (a) 1.8 m/min; (b) 2.4 m/min e (c) 3.0 m/min

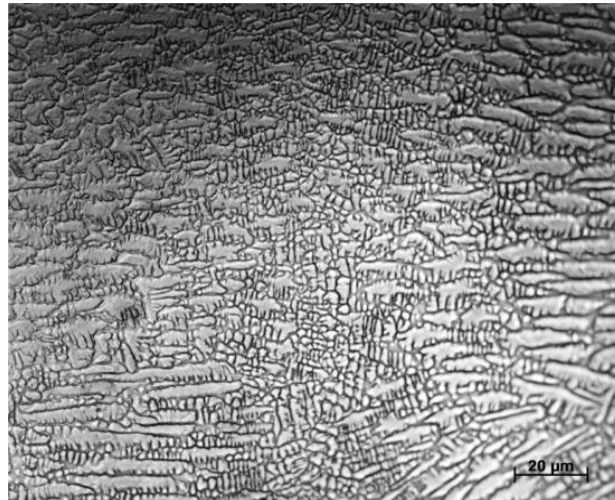


Fig. 3: Microstructure observed at the center of the bead. Speed 1.8 m/min

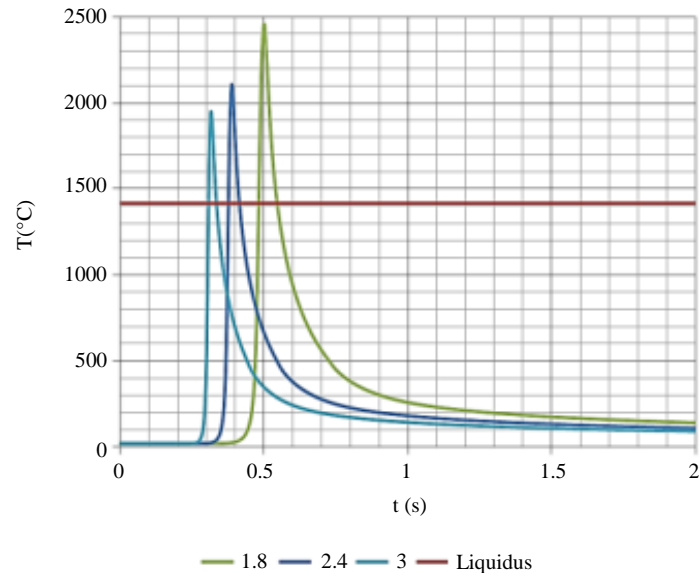


Fig. 4: Prediction of the temperature as a function of the time in the center of the welds according to SysWeld software. Room temperature laser welding for welding speeds: 1.8, 2.4 and 3.0 m/min. The liquidus line is represented as well

Quenching and Aged Welds

Quenched and aged welds are those heat-treated subsequent to complete quenching, as presented in Fig. 6. The temperature profile came from Sysweld simulation (laser weld) and from the thermocouple records when the time is above 10 seconds. For the welding, only one condition (3 m/min) had been chosen, although the time and temperature for isothermal aging was changed. Figure 6 also presents the temperatures for austenite reversion in heating (Ah) and Martensitic transformation in Cooling (Mc). The isothermal aging was conceived to occur between the Ah and Mc lines, in accordance to previous works (Fanton *et al.*, 2014).

Figure 7 presents the macroographies of the welded regions and surroundings as a function of the aging time and temperature. The weld shapes resemble those obtained in ambient temperature conditions (Fig. 2), although the penetration attained the bottom surface in a majority of cases. Since the furnace configuration does not support a protective gas nozzle, the enhanced weld penetration could be associated to a better plasma coupling or to the absence of surface cooling induced by the flowing argon. Also, the HAZ is more distinctive in Fig. 7 compared to Fig. 2 because of precipitation of intermetallic compounds.

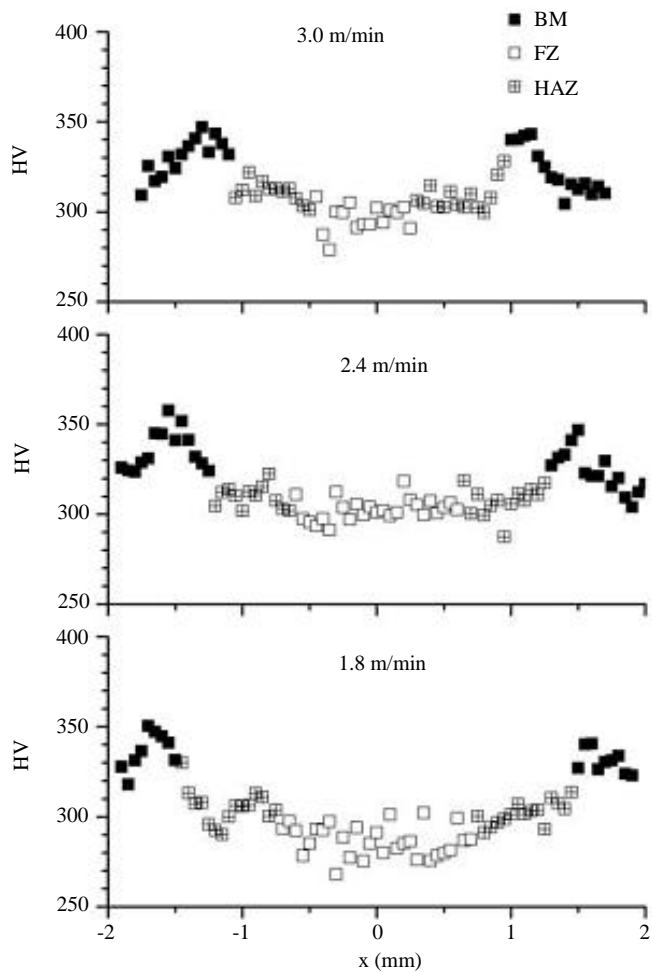


Fig. 5: The Vickers hardness profiles of the welds obtained in different speeds at room temperature. The FZ, HAZ and BM are indicated by different symbols

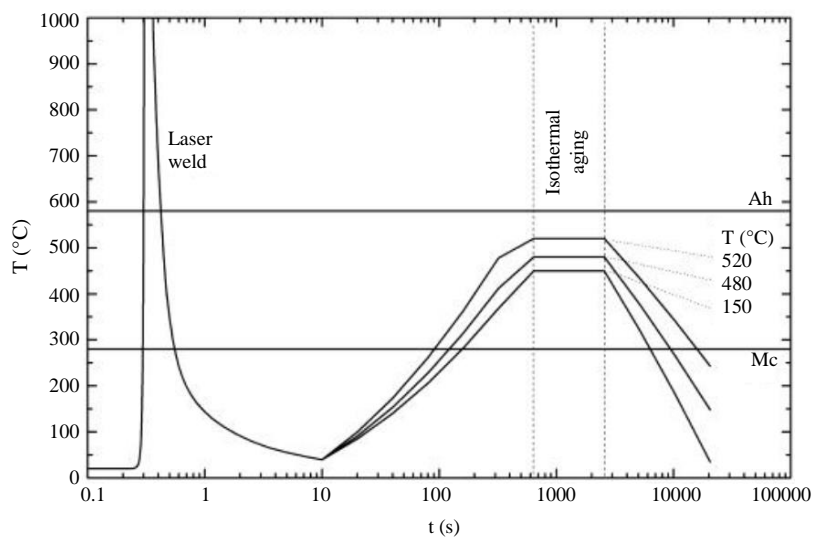


Fig. 6: The temperature profile for the quenched and aged. Although the isothermal period was changed from 10 to 30 min, only the 30 min. isotherm is shown. The time is plotted in logarithm scale for clearness

The intermetallic precipitation noticed for the ambient temperature welds (Fig. 3) is still visible in the welds after aging (Fig. 8a). Although a partial solubilization of the microsegregation after an aging of 520°C per 10 min promoted a skeleton-type distribution. The aged martensite is also visible in Fig. 8a, with the precipitates removed by the chemical etching. Figure 8b shows a region near the Fusion Line (FL) where the same features of the weld centerline could be seen at the right. At the left, aged martensite grains are free of massive precipitates as those observed in the FZ.

The hardness profiles for each aging condition are plotted in Fig. 9 as a function of the region: FZ, HAZ and BM. As reported before (Sakai *et al.*, 2015), the general tendency is an increase in HV when increasing aging time or the temperature. However, the FZ values are distinctly below the other regions HV. As presented before, Fig. 8, the heat treatment was not sufficient to homogenize the as-solidified precipitates at the interdendritic region. Some important elements for nucleation during aging, particularly Ti and Mo, are depleted in the martensite matrix and therefore the FZ

tempered martensite is softer than other regions. The hardness obtained in BM and HAZ are the same because of the initial homogeneous structure.

After 30 min the average hardness of BM and HAZ attained approximately 510, 520 and 570 HV for temperatures of 450, 480 and 520°C, respectively. For the same temperatures the FZ attained considerably lower values of 440, 470 and 490 HV, respectively.

Intercritical Aging

Instead of quenching and aging the laser welded coupons, the intercritical aging aimed to heat the steel plated between Mc and Ah in order to create a duplex structure $\alpha+\beta$ (Fig. 1). Figure 10 is a time-temperature plot composed of Sysweld results (laser weld) and the thermocouple record data (heating, isothermal aging and cooling). The temperature path was chosen slightly above the previous temperatures (Fig. 7) to maximize diffusion of the elements, but keep it below the austenite reversion on heating. The average isotherm is 570°C, with a little period above Ah due to the laser heat input.

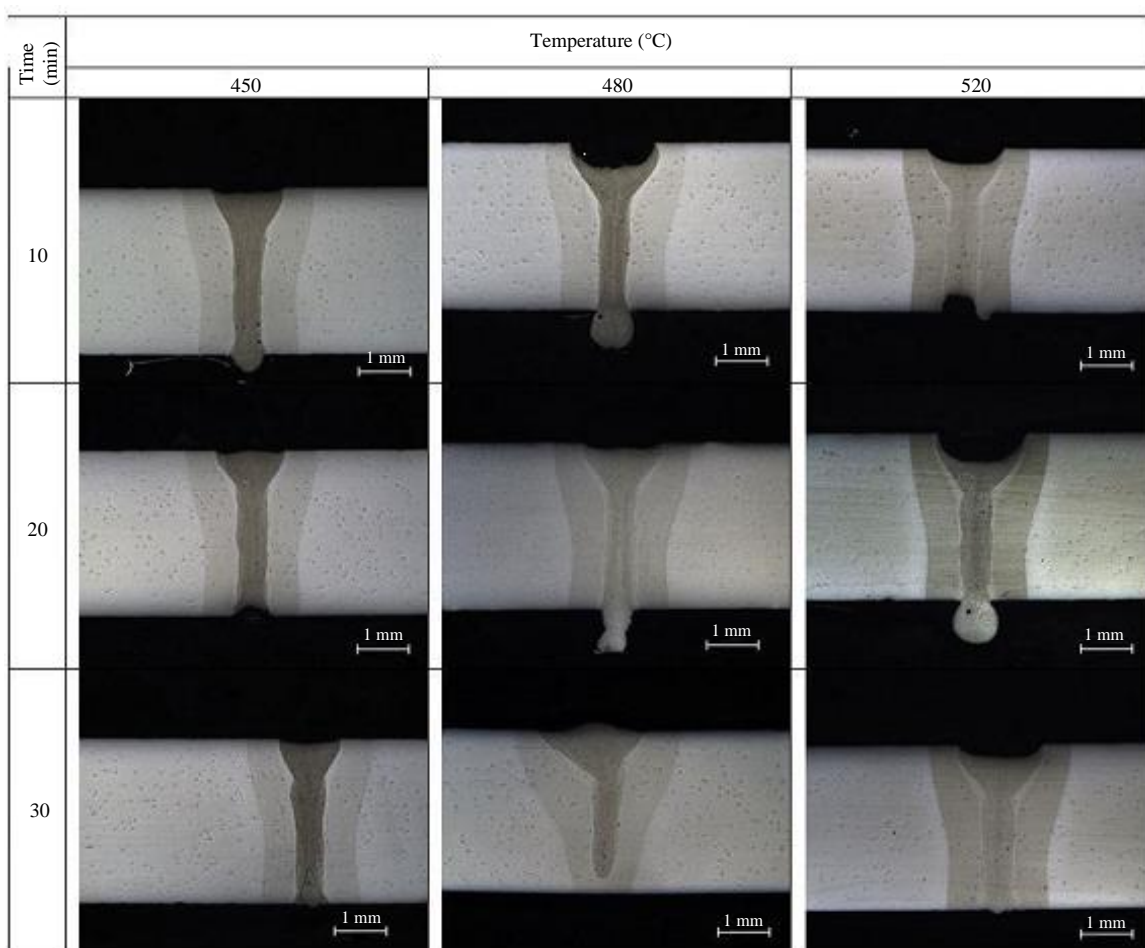


Fig. 7: General view of the cross section macrographs obtained in different aging temperatures and times

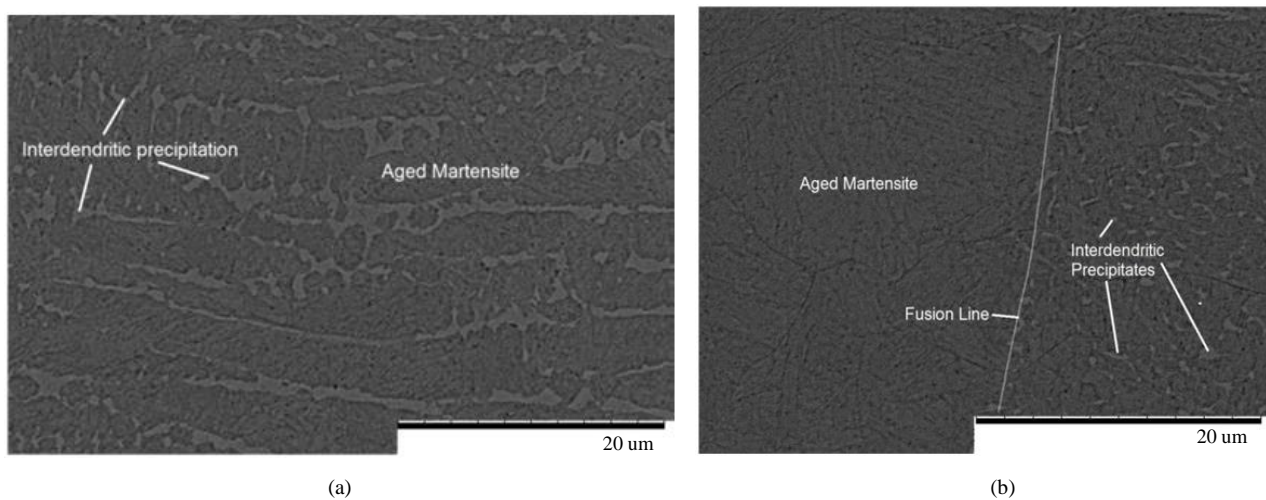


Fig. 8: Central region of the FZ (a) and the HAZ (b) for the welded and aged sample (520°C/10 min)

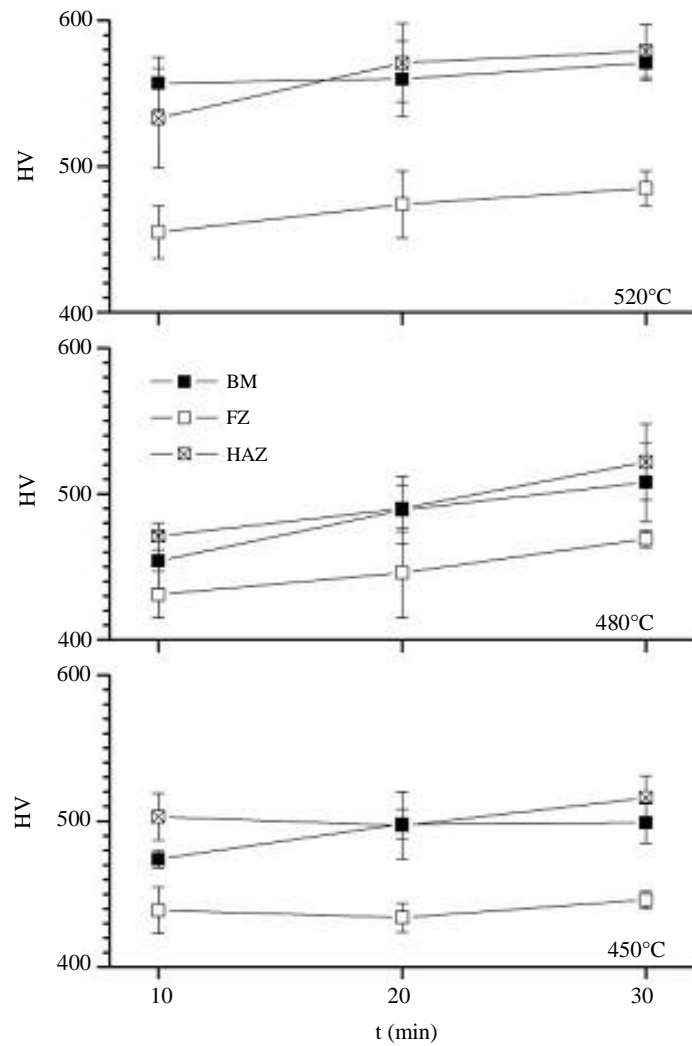


Fig. 9: Plots of the hardness profiles for the welded and aged samples

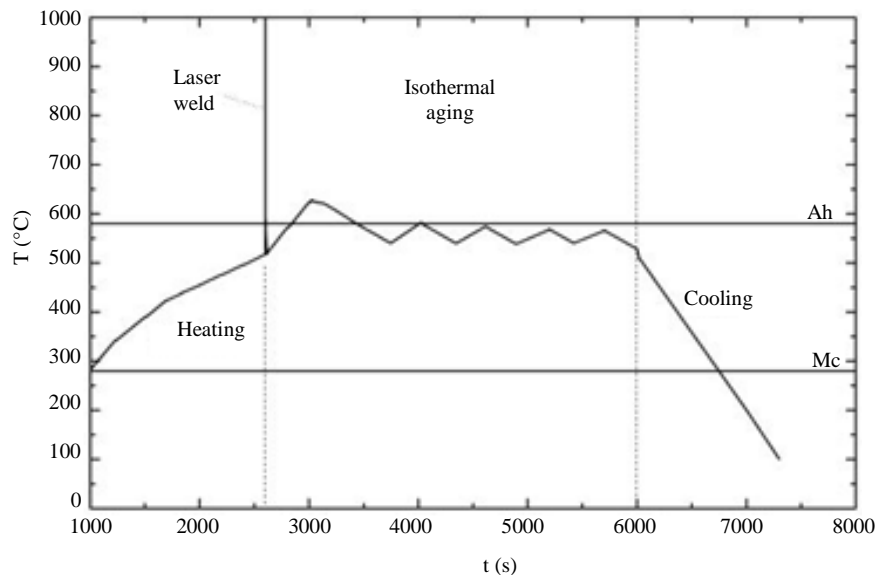


Fig. 10: Temperature evolution as a function of the time according to sysweld (weld) and a thermocouple record. Isothermal fixed at 570°C

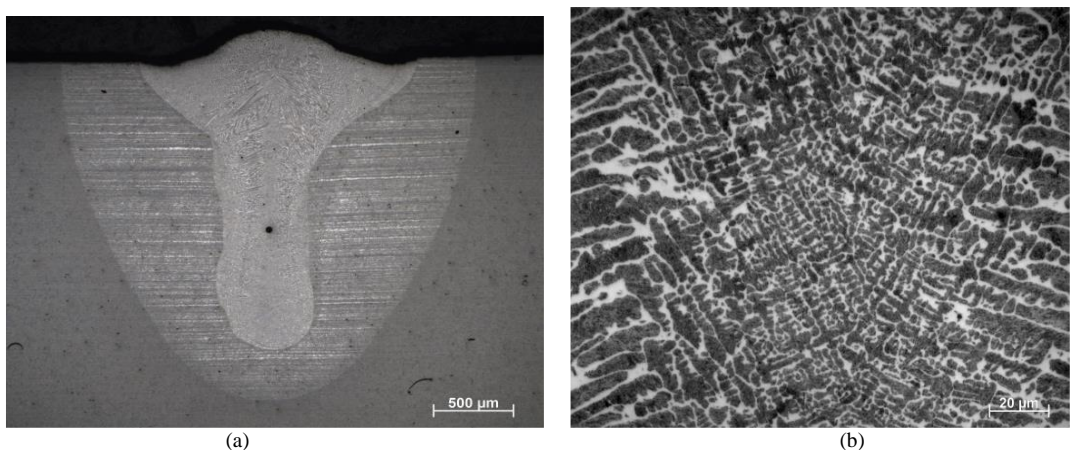


Fig. 11: (a) Macrostructure of in-situ aged weld and (b) microstructure at the middle of the FZ

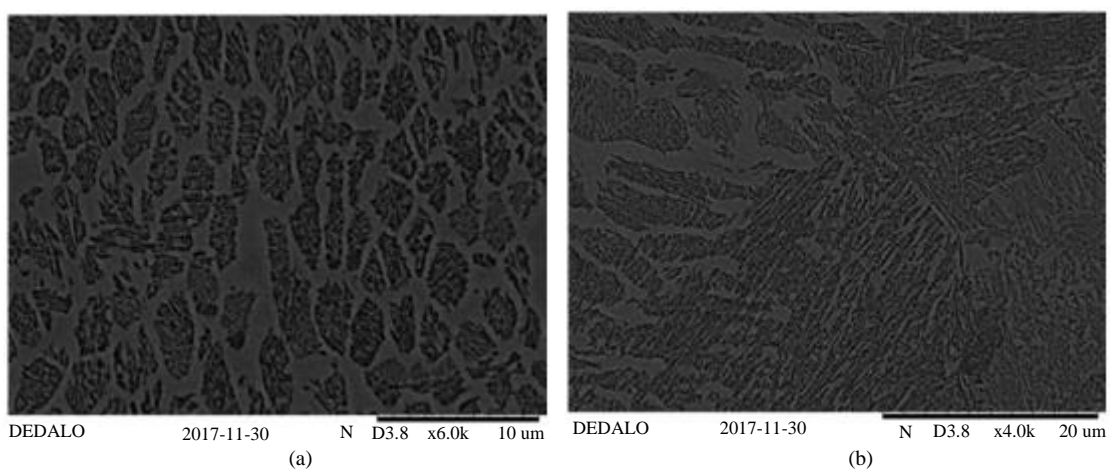


Fig. 12: Scanning electron microscopy (a) the microstructure near to the center of the FZ and (b) FZ/HAZ interfac

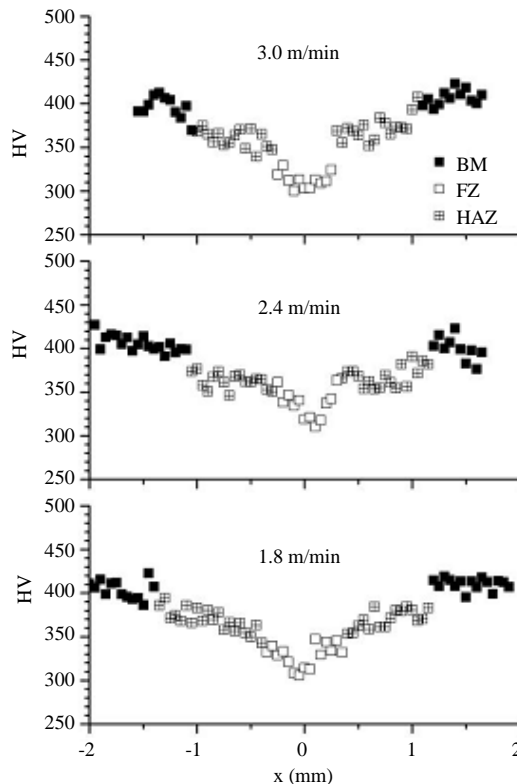


Fig. 13: The Vickers hardness profiles of the welds obtained in different speeds after in-situ aging. The FZ, HAZ and BM are indicated by different symbols

The weld macrostructure (Fig. 11a) and FZ microstructure (Fig. 11b) is very different from previous observations. The entire coupon was heat treated creating a flatter etching contrast (Fig. 11a). The FZ microstructure is composed by a light gray (ferrite) and dark gray (martensite) phases with calculated surface phase amounts of 43% ferrite and 57% martensite. Scanning electron images (Fig. 12a) indicated the ferrite phase occupies the former interdendritic spaces growing at expense of microsegregated phases. Figure 12b is an image obtained near to the fusion line of the weld. In the figure, the HAZ ferrite growth occurred with a Widmanstätten morphology from the grain boundaries.

The hardness of the coupons (Fig. 13) lay between the room temperature welds (Fig. 5) and welded and aged samples (Fig. 9). The hardness range of all welding speeds was narrower than the welds without heat treatment, which could eventually lead to a decrease in stress concentrators.

Conclusion

This work compared the microstructure and hardness of maraging 300 plates obtained from room temperature

weld, quenching and aging and intercritical aging with the use of a furnace coupled to a laser workstation.

The microstructure of room temperature welds is marked by dendrite growth, hence they present some microsegregation. This solute partitioning is responsible for the depletion in hardness in the weld compared to surrounding regions. The Fusion Zone (FZ) hardness situated between 280 and 300 HV, consistent with an unaged martensite structure. The Heat-Affected Zone (HAZ) hardness are typically above the FZ Vickers hardness because of the solid-state transformation implies in the absence of microsegregation. Finally, the Base Material (BM) is delimited by the temperature below the austenite reversion on heating.

When the welded coupons were quenched and aged in the range of temperatures 450 to 520°C, with times from 10 to 30 min, the aged martensite was observed. After 30 min the average hardness of BM and HAZ attained approximately 510, 520 and 570 HV for temperatures of 450, 480 and 520°C, respectively. For the same temperatures the FZ attained considerably lower values of 440, 470 and 490 HV, respectively, due to the composition modulation.

Using an intercritical aging, the hardness situated between room temperature and quenched and aged coupons and are more homogeneous considering fusion zone, heat affected zone and base material. The microstructure of the intercritical aged welds is marked by duplex-ferrite and martensite microconstituents. The hardness range of all welding speeds was narrower than the welds without heat treatment, which could eventually lead to a decrease in stress concentrators.

Acknowledgment

This research has been supported by Fundação de Amparo à Pesquisa do Estado de São Paulo (FAPESP) under grant number 2016/16683-8.

Author's Contributions

Milton Sergio Fernandes de Lima: Managed the research and wrote the paper.

Rafael Humberto de Mota Siqueira: Conceived and designed the analysis; Performed the laser experiments.

Sheila Medeiros de Carvalho: Collected the simulation data; Performed the microstructural analysis.

Antonio Jorge Abdalla: Contributed analysis tools; Performed the mechanical analysis.

Ethics

The authors have declared no ethical issue of the publication of the present paper.

References

- Andersson, J.O., T. Helander, L. Höglund, P.F. Shi and B. Sundman, 2002. Thermo-calc and DICTRA, Computational tools for materials science. *Calphad*, 26: 273-312. DOI: 10.1016/S0364-5916(02)00037-8
- ASM Handbook Committee, 1990a. Properties and Selection: Irons, Steels and High-Performance Alloys. 10th Edn., ASM, Metals Park (OH), ISBN-10: 0871703777, pp: 1063.
- ASM Handbook Committee, 1990b. Heat Treating. ASM, Metals Park (OH).
- Bieber, C.G., 1969. Nickel Alloy. US. Patent No. 3,093,518, Filed Setember 11.
- Braga, V., R.A.F. Mansur, R.H.M. Siqueira and M.S.F. Lima, 2018. Formability of in-situ austempered transformation-induced plasticity steels after laser beam welding. *Soldagem Inspeção*, 23: 402-412. DOI: 10.1590/0104-9224/si2303.09
- Casati, R., J.N. Lemke, A. Tuissi and M. Vedani, 2016. Aging behaviour and mechanical performance of 18-Ni 300 steel processed by selective laser melting. *Metals*, 6: 1-13. DOI: 10.3390/met6090218
- ESI-group, 2019. ESI-group Sysweld Software.
- Fanton, L., A.J. Abdalla and M.S.F. Lima, 2014. Heat treatment and yb-fiber laser welding of a maraging steel. *Weld. J.*, 93: 362-368.
- Joseph, A., H. Enguang, L. Chen, J. Dear and C. Davies, 2017. The effect of Ar and He shielding gas on fibre laser weld shape and microstructure in AA 2024-T3. *J. Manufac. Process.*, 29: 62-73. DOI: 10.1016/j.jmapro.2017.07.011
- Kapoor, R., L. Kumar and I.S. Batra 2003. A dilatometric study of the continuous heating transformations in 18wt.% Ni maraging steel of grade 350. *Mater. Sci. Eng. A*, 352: 318-324. DOI: 10.1016/S0921-5093(02)00934-6
- Kellogg, B., 2012. Friction stir welding and post-weld heat treating of 250-grade maraging steel. South Dakota School of Mines, Research Experience for Undergraduates, National Science Foundation.
- Krasnikova, S.I., S.B. Vukelich, A.V. Drobot and A.Y. Shmelev, 1986. Dendritic inhomogeneity of stainless maraging steels. *Mater. Sci. Heat Treat.*, 27: 781-786.
- Lahdo, R., O. Seffer, A. Springer, S. Kaierle and L. Overmeyer, 2014. GMA-laser hybrid welding of high-strength fine-grain structural steel with an inductive preheating. *Phy. Proc.*, 56: 637-645. DOI: 10.1016/j.phpro.2014.08.060
- Lima, M.S.F., D. Gonzales and S. Liu, 2017. Microstructure and mechanical behavior of induction assisted laser welded AHS steels. *Weld. J.*, 96: 376-388.
- Linnert, G.E., 1967. Welding Metallurgy Carbon and Alloy Steel. 3rd Edn., AWS, New York, ISBN-10: 0686956052.
- Lombardo, S., R.N. Ferreira, L.A.S. Santos, J.W.J. Silva and V. Scheid *et al.*, 2016. Microstructural characterization of joints of maraging 300 steel welded by Laser and subjected to plasma nitriding treatment. *Mater. Sci. Forum*, 869: 479-483. DOI: 10.4028/www.scientific.net/MSF.869.479
- Pektas, I. and H. Atala, 1998. The effects of various heat treating parameters on the hardness and microstructures of the experimental 18% nickel maraging steels. *J. Thermal Analy.*, 54: 803-814. DOI: 10.1023/A:1010191820258
- Rajkumar, V., N. Arivazhagan and R.K. Devendranath, 2014. Studies on welding of maraging steels. *Proc. Eng.*, 75: 83-87. DOI: 10.1016/j.proeng.2013.11.017
- Rohrbach, K. and M. Schmidt, 1993. Maraging Steels. In: *ASM Metals Handbook: Properties and Selection: Irons, Steels and High-Performance Alloys*. 2nd Edn., ASM International, Ohio.
- Sakai, P.R., M.S.F. Lima, L. Fanton, C.V. Gomes and S. Lombardo *et al.*, 2015. Comparison of mechanical and microstructural characteristics in maraging 300 steel welded by three different processes: LASER, PLASMA and TIG. *Proc. Eng.*, 114: 291-297. DOI: 10.1016/j.proeng.2015.08.071
- Sha, W., 2000. Thermodynamic calculations for precipitation in maraging steels. *Mat. Sci. Technol.*, 16: 1434-1436. DOI: 10.1179/026708300101507415
- Silva, J.J.M., I.F. Vasconcelos, F.I.S. Silva, T.S. Ribeiro and H.F.G. Abreu, 2019. An atomic redistribution study of the 440°C ageing kinetics in maraging-300 steel. *Mater. Res.*, 22: 1516-1439. DOI: 10.1590/1980-5373-mr-2018-0230
- SAE Mobilus, 2019. Steel, maraging, bars, forgings, tubing and rings 18.5Ni -9.0Co -4.9Mo -0.65Ti -0.10Al Consumable Electrode Vacuum Melted, Annealed (AMS6514 Aerospace Material Specification)-SAE Mobilus.